Available online at www.sciencedirect.com
ScienceDirect
International Journal of Heat and Mass Transfer 50 (2007) 5108–5123
International Journal of HEAT and MASS TRANSFER
www.elsevier.com/locate/ijhmt

Heat transfer characteristics of an impinging inverse diffusion flame jet – Part I: Free flame structure

L.L. Dong [a,b,*], C.S. Cheung [b], C.W. Leung [b]

[a] Institute of Sustainable Energy Technology, School of the Built Environment, University of Nottingham, UK
[b] Department of Mechanical Engineering, The Hong Kong Polytechnic University, Hong Kong, China

Received 22 March 2007; received in revised form 25 June 2007
Available online 11 September 2007

Abstract

This is the first part of the experimental investigation on the feasibility of inverse diffusion flame (IDF) for impingement heating. This part is aimed to identify the favorable IDF structure for impingement heating. Seven IDF structures have been observed altogether. Among them the favorable flame structure for impingement heating is identified to comprise a short base diffusion flame and a long premixed flame torch, separated by a contracted flame neck, which acts as a mixing zone for air and fuel and stabilizes the premixed flame torch. This unique flame structure allows the IDF to possess the advantages of both premixed and diffusion flames, with no flashback, high flame temperature and less or no soot emission. The emission measurement shows it emits low level of nitrogen oxides. Its favorable thermal structure and emission characteristics make it a desirable option for impingement heating.

Keywords: Inverse diffusion flame; Flame structure; Combustion emission

1. Introduction

Impinging flame jets have been widely used in industrial and domestic heating applications for their enhanced convective heat transfer rates [1–3]. The thermal performance of a flame impingement system is dependent significantly on four factors: burner style, flame jet properties, impingement surface condition, and configuration between burner nozzle and surface. Extensive literature reviews on impinging flame jets have been carried out by Viskanta [4,5], Baukal and Gebhart [6–9] and Chander and Ray [10]. Comparing to normal diffusion flame (NDF), premixed or partially premixed flames are normally used for impingement heating because of high flame temperature and soot-free flame structure. Structures and heat transfer characteristics of a single or an array of two or three laminar or turbulent premixed flame jet have been studied by several researchers [11–15]. A cold central core with low heat flux around the stagnation point is found by several investigators [16–18]. Kataoka et al. [19] and Kataoka [20] found that the maximum heat transfer occurs at the stagnation point when the nozzle-to-plate distance is equivalent to the jet potential core length when combusted methane/air gases impinge upwards normally on a flat plate. Hargrave et al. [21,22] investigated the flame structure and heat transfer characteristics of a turbulent premixed methane/air flame jet. van der Meer [23] investigated the heat transfer characteristics of a turbulent natural gas/air impinging flame jet with both experimental and numerical methods. The effects of the nozzle-to-plate angle on the heat transfer characteristics have been investigated by Kremer et al. [24] and Dong et al. [25]. Tuttle et al. [26,27] investigated experimentally both the time-averaged and time-resolved heat transfer characteristics of a single impinging partially premixed methane/air flame jet. An array of two or three impinging premixed flame jets have

* Corresponding author. Address: Institute of Sustainable Energy Technology, School of the Built Environment, University of Nottingham, UK.
E-mail address: leilei.dong@nottingham.ac.uk (L.L. Dong).

0017-9310/$ - see front matter © 2007 Elsevier Ltd. All rights reserved.
doi:10.1016/j.ijheatmasstransfer.2007.07.018

Nomenclature

d	diameter (m)
L	flame height (m)
r	radial distance from stagnation point (m)
Re	Reynolds number ($= u_{air}d_{air}/v_{air}$)
T	temperature (K)
u	gas velocity (m/s)
y	axial distance from the burner exit (m)

Greek symbols

v	kinematic viscosity (m^2/s)
Φ	equivalence ratio (=(stoichiometric air/fuel volume ratio)/(actual air/fuel volume ratio))

Subscripts

air	air jet
f	flame jet
inner	flame inner cone
outer	flame outer layer

been investigated by Dong et al. [28,29] and Chander and Ray [30]. Malikov et al. [31] studied numerically heat transfer in a rapid heating furnace with a multi-jet combustion chamber. Besides the predominant research interests in the premixed or partially premixed impinging flame jets, other flame types have also been investigated previously. The thermal and pollutants emission characteristics of a single and a row of two or three radial jet reattachment flame jets have been studied by Mohr et al. [32], Seyed-Yagoobi et al. [33] and Wu et al. [34]. The flame structure and heat transfer characteristics of an impinging diffusion flame jet have been investigated by Rigby and Webb [35].

While a premixed or partially premixed flame jet can produce intense heat release rate and high flame temperature and soot-free flame structure, it has the intrinsic danger of flashback. Therefore, additional device is necessary to prevent the flame flashback. Furthermore, premixed or partially premixed flames are easy to blow off without external stabilization facilities. In most cases, a turbulent flame jet needs pilot flames to stabilize [36,37]. The introduction of both external facilities complicates the burner design. Although normal diffusion flame has a good combustion safety and low tendency to blow off, it suffers from low heat release rate, excess soot emission, and over-long flame length due to incomplete combustion. Therefore, it is not a desirable option for impingement heating purpose.

To bypass the shortcomings of both the premixed and diffusion flames and take advantage of the both, the inverse diffusion flame jet is a possible alternative. The IDF is formed when the central oxidizer is discharged into the surrounding fuels. Previous studies concentrated on the IDF produced by the co-flowing fuel and oxidizer where the flame was mainly yellow in appearance due to incomplete mixing. It is convenient to use this type of IDF to study soot evolution because carbon-containing species forming on the fuel side of the flame can convect out without passing through the oxidizing flame tip [38–40]. Some researchers found that the IDF is capable of achieving ultra-low levels of NO_x to less than 18 ppm [41,42]. However, most IDFs studied before are not suitable for impingement heating because of the yellow flame appearances with excess soot emission. Moreover, little study has been performed on the application of the IDF for impingement heating. Therefore, the present investigation is motivated to identify the favorable IDF structure and explore the feasibility of the IDF for impingement heating as a desirable alternative to premixed or partially premixed flame jets. The preferable IDF for impingement heating purpose should meet several crucial criteria including high flame temperature, blue flame appearance with less or no soot emission, and acceptable pollutants emission level. Bearing them in mind, the thermal structure and emission properties of a free IDF are investigated as a basis for impingement heat transfer study in the first part of this paper. The heat transfer characteristics of the impinging IDF will be presented in the second part of this paper.

2. Experimental test rig and methods

The experimental setup is shown schematically in Fig. 1. The IDF was produced by a perforated brass burner with a 6-mm diameter air port in the center surrounded by a row of 12 evenly distributed fuel ports of 2.4 mm in diameter. The center-to-center distance between the central air port and each fuel port is 8 mm. Metered air was directly delivered to the IDF burner, while the metered butane gas was divided into two lines to enter the settling chamber in opposite directions. The distance between the inlets of the fuel gas is 40 mm. The opposite entry of the fuel gas is designed to obtain high level of turbulence before exiting. The augmented free stream turbulence will enhance the mixing of the fuel with the air after being issued. The IDF burner was fixed on a three-dimensional positioner which could be moved freely. The IDF was enclosed with screen mesh to minimize the disturbance of the surrounding air flow. Gas samples within the flame were extracted by a quartz tube with an inner diameter of 1 mm and outer diameter of 2 mm, which is connected with a long flexible tube in the other end to cool the sampled gas flowing inside before entering into the gas analyzers.

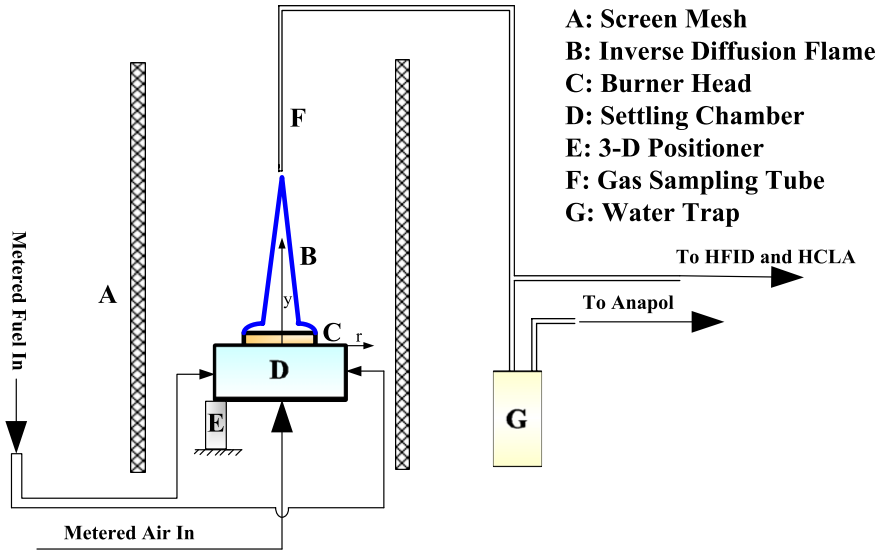

Fig. 1. Schematic of the experimental setup.

The flame temperature was measured by a B-type uncoated bare wire thermocouple. The thermocouple was fixed on a still holder. By moving the burner, the radial and axial flame temperature distributions were measured. A stand-alone IOtech data acquisitor was used to record the temperature. Each temperature measurement reported here is the rms value of data taken consecutively in 10 s at a rate of 1000 samples/s. Corrections are made for temperatures over 300 °C to compensate for the radiative and convective heat exchanges from the thermocouple bead with the method suggested by Bradley and Matthews [43]. The emissivity of the thermocouple bead is assumed to be a constant since no soot accumulation is found in the present study. An emissivity of 0.14 is selected as recommended for uncoated Type B thermocouple by Sparrow and Cess [44]. The maximum temperature corrected is 118 °C. Direct images of the flames were obtained with a digital camera. An Anapol gas analyzer was employed for CO, CO_2, and O_2 measurements. A heated flame ionization detector (HFID) was used to measure the concentration of HC. NO/NO_x measurement was performed with a heated chemiluminescent analyzer (HCLA).

Experiments were designed and conducted in order to provide a full picture of the flow patterns and flame structures of IDF from a port-array burner. It is in the authors' intention to find out the desirable burner operating range for heating purpose with high flame temperature and without much emission penalty. Therefore, the Reynolds number of air jet in the present investigation stretches from zero to an upper limit where flame blows out. The global overall equivalence ratio, O, varies from zero to a critical value where yellow plume dominated flame starts to form. The research emphasis is given to the IDF in the ascertained desirable operating range where it is blue, double-structured, and possessing three flame layers.

3. Calculation procedure and error analysis

The co-ordinate system used in the present study is also shown in Fig. 1. To ensure the repeatability, each run of experiments was conducted two times and the averaged values are reported and employed to perform the error analysis. The uncertainty analysis was performed with the method of Kline and McClintock [45]. With 95% confidence level, the minimum and maximum uncertainties in the flame temperature measurements are 2.6% and 10.4%, respectively. The uncertainty of the HC measurement ranges between 1.7% and 8.2%. The minimum and maximum uncertainties of CO measurement are 2.1% and 9.5%, respectively. The uncertainty of the NO measurement ranges from 2.3% to 12.3%. The minimum uncertainties of CO_2 and O_2 are 1.1% and 1.3%, respectively, while their maximum uncertainties are 8.3% and 9.2%, respectively.

4. Results and discussion

4.1. Flow aerodynamics and flame structures

It has been found that fuel/air jet entrainment is a crucial factor determining the flow and flame structures of the concentric co-flowing IDF. The effects of entrainment have been discussed in detail elsewhere [46,47]. For a port-array burner produced IDF, the air and fuel jets are located some distance away between each other; the between-jet entrainment could be too weak to exert decisive effect on the hydrodynamics of the air and fuel jets.

In fact, for the system of multiple jets issuing from a port-array burner, the flow field is very complicated. Basically, two types of flow structure have been found in our experiments, according to the level of interference between the air and fuel jets. Firstly, when the interference is weak,

the air and fuel jets develop separately with each behaving as a single jet. Secondly, when the interference becomes strong enough, the fuel jets will be sucked to the sub-atmospheric pressure zone formed near the air jet, and deflect inwards and impinge on the air jet. Fuel jet impingement greatly enhances the mixing of air and fuel. After the mixing, the gas mixture develops further as a single flame jet. When the mixing level is high enough, a premixed flame could be formed and propagates downstream. For this jet impingement configuration, the intense mixing process could also increase chemical reaction rate and combustion efficiency, as discussed by Bain and Smith [48]. The reaction rate was found to be proportional to the flow intensities by Holve and Sawyer [49] and Witze [50].

It is found in the present study that Re_{air} and the ratio of the velocity of air to fuel jet (or, the O), are two key factors influencing the level of the between-jet interference. For fixed air jet diameter, the Re_{air} is proportional to the air jet velocity. It is found that a critical value of Re_{air} exists defining the between-jet interference. When Re_{air} is below this value, it is not able to change the trajectory of the surrounding fuel jets regardless of O. When Re_{air} exceeds this value, the impingement of the fuel jets could happen depending on O. When Φ is lower than a critical value, the velocity difference between the air and fuel jets is large enough to alter the fuel jet flow. Beyond that, the relatively small velocity difference is not able to cause the deflection and impingement of the fuel jets. In this case, the air and fuel jets behave again as separate jets.

By varying Re_{air} and Φ, seven typical flame shapes are found in the present experiments, as shown from Figs. 2a–g. Their corresponding flame structures are illustrated from Figs. 3a–g. The operating range of the IDF and the critical values of Re_{air} and Φ to separate different flame structures are shown in Fig. 4.

Fig. 2a. Buoyancy-driven yellow tip IDF.

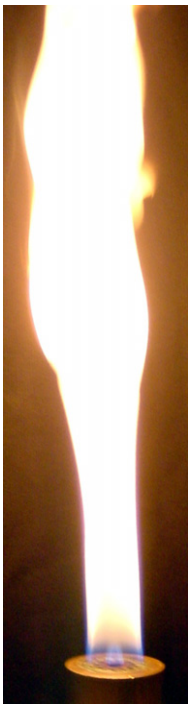

Fig. 2b. Buoyancy-driven yellow plume IDF.

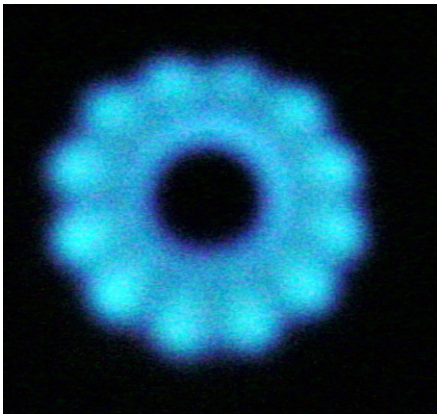

Fig. 2c. Blue ring IDF (top view).

When Re_{air} is lower than 300, the flame is blue at the root of the flame and yellow elsewhere, which appears to be a typical buoyancy-driven diffusion flame as described elsewhere [51]. Due to the low Re_{air}, the between-jet interference is negligible, thus the flame exhibits two layers of blue flame appearing close to the air and fuel exits, as shown in Figs. 2a and 2b and illustrated schematically in Figs. 3a and 3b, respectively. These two flame surfaces correspond to interface between the fuel and the air. The surface of the inner diffusion blue flame is where air from the central jet and the fuel meet each other with Φ equal to 1.0. The front of the outer blue flame is formed at the

Fig. 2d. Open blue IDF.

Fig. 2e. Blue dual-structure triple-layer IDF.

Fig. 2f. Momentum-controlled yellow tip IDF.

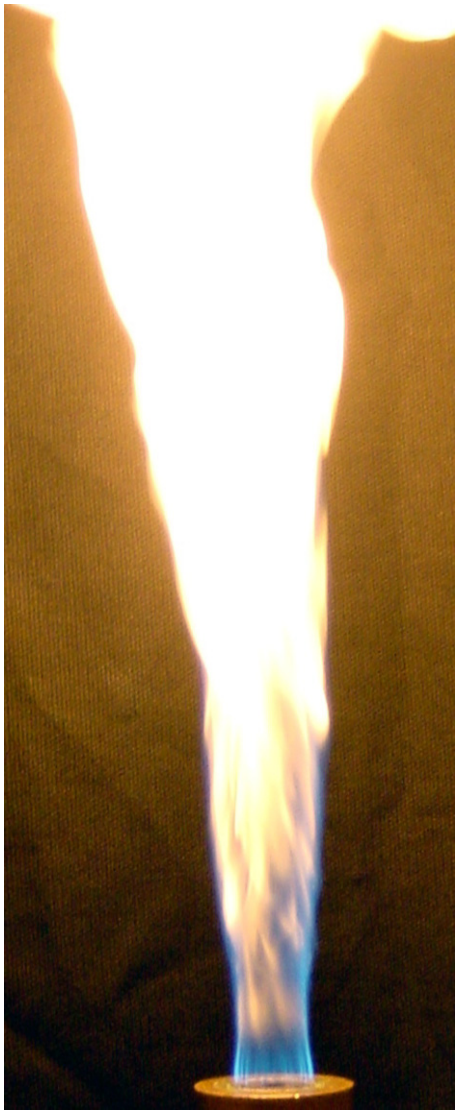

Fig. 2g. Momentum-controlled yellow plume IDF.

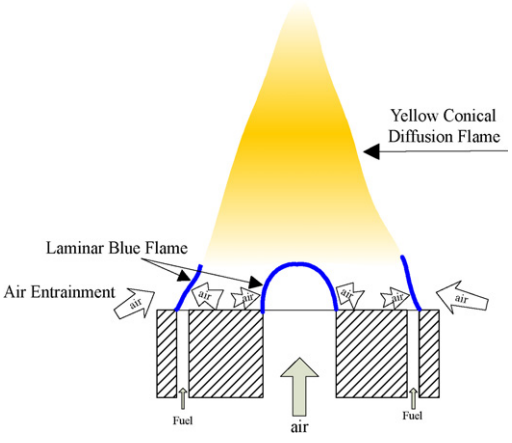

Fig. 3a. Structure of buoyancy-driven yellow tip IDF.

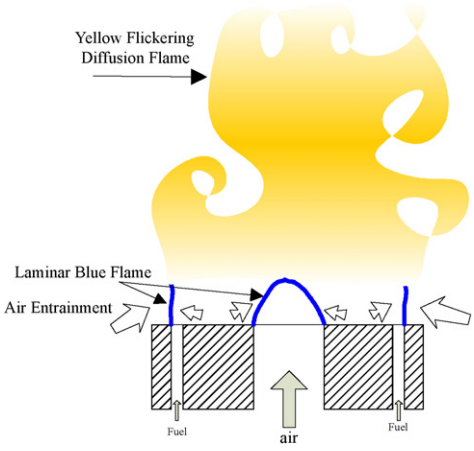

Fig. 3b. Structure of buoyancy-driven yellow plume IDF.

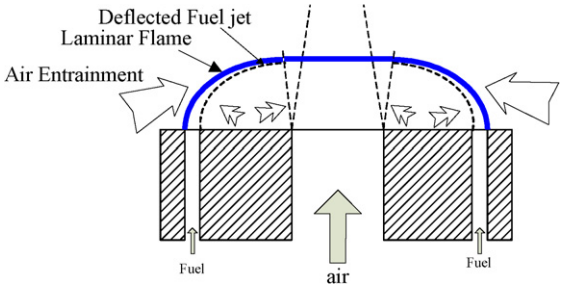

Fig. 3c. Structure of blue ring IDF.

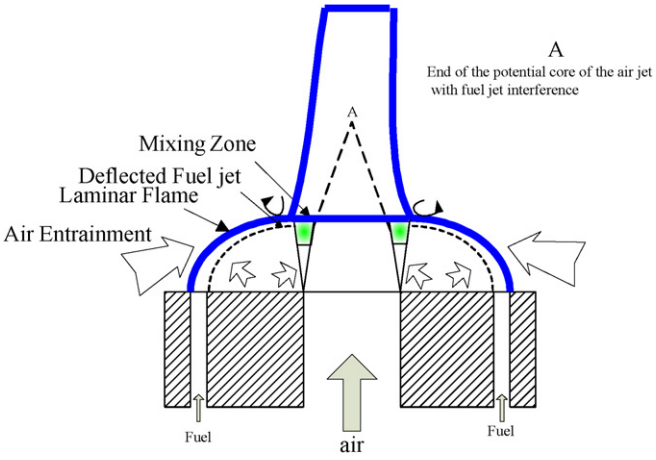

Fig. 3d. Structure of blue open IDF.

interface between the fuel jets and the surrounding air. No interference between the air and fuel jets is observed. This double-layer flame structure is also found by Hamins et al. [52] and Huang et al. [53].

When Φ is lower than 1.5, it is a stable yellow laminar diffusion flame with a conical shape formed due to flame stretch effect, as shown in Fig. 2a. Beyond that, the flame tip starts to flicker due to the buoyancy effect, and finally develops into a yellow plume, as shown in Fig. 2b. The conical shape is destroyed at higher value of Φ because of

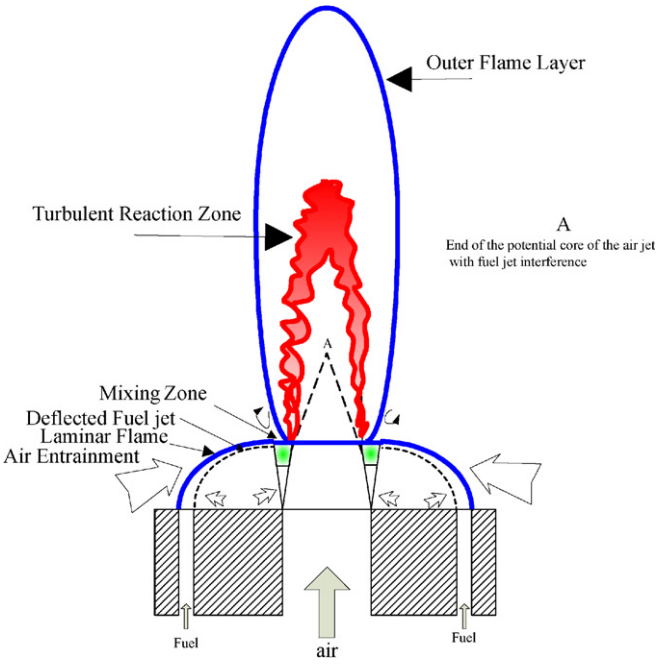

Fig. 3e. Structure of blue dual-structure triple-layer IDF.

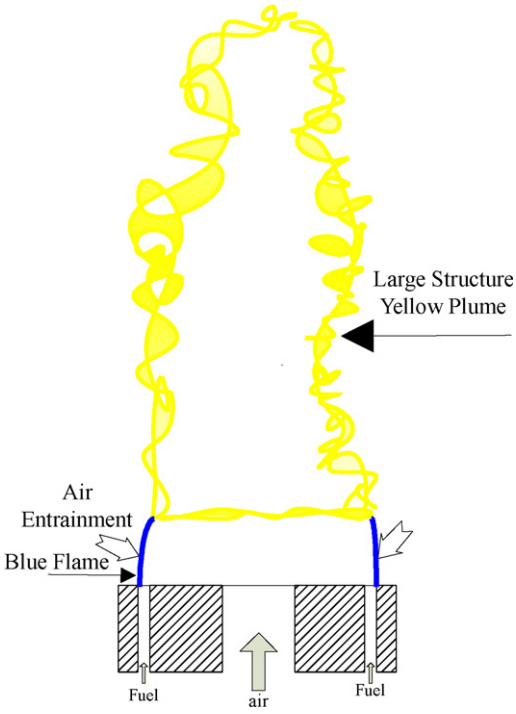

Fig. 3g. Structure of momentum-controlled yellow plume IDF.

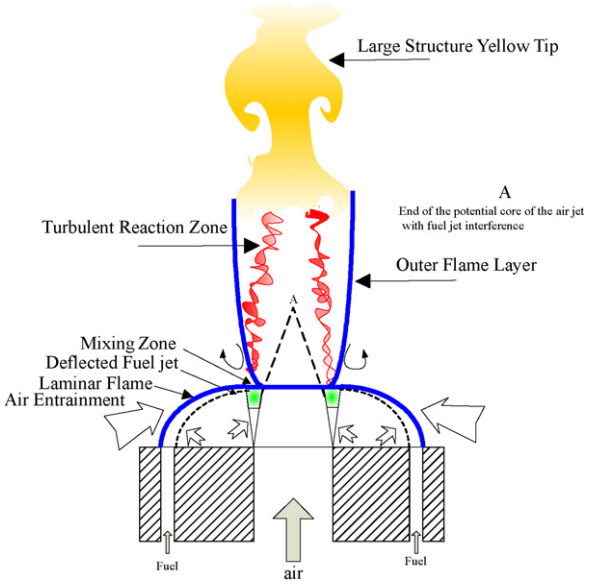

Fig. 3f. Structure of momentum-controlled yellow tip IDF.

the weakened flame stretch effect. The entrainment of ambient air into the fuel jet increases with fuel velocity, resulting in the increased mixing of the fuel and the surrounding air. Thus, the flame stretch effect is weakened. The characteristics of this buoyancy-induced flame flickering can be referred to elsewhere [54]. Shu et al. [55] attributed the buoyancy-driven yellow plume to the effect of buoyant acceleration of hot gases outside the diffusion outer flame layer, which causes shear-layer rollup, leading to the formation of toroidal vortex rings in the plume.

When Re_{air} exceeds 300, the flame becomes momentum-controlled and is characterized by the appearance of a contracted flame neck. In this condition, Re_{air} is large enough to be able to suck the surrounding fuel jets and thus alter the flow field and flame structure. At this transitional point, the Froude number of air jet (Fr_{air}) is 2.55, which also suggests the dominance of the momentum-controlled mechanism. The flame remains stable until Re_{air} reaches 8000. Within this stable range, two distinct flame structures are identified. When Re_{air} is less than 4000, the flame is characterized by a yellow ring appearing close to the neck of the flame when Φ is lower than a certain value. Beyond that, the yellow ring disappears and a fully blue flame could be formed. This yellow ring is an indicator of soot emission, which is formed due to incomplete mixing of air and fuel as a result of less intense between-jet interference. The soot forms in the fuel-rich region in the fuel side, characterizing the IDF with a yellow ring close to the neck.

Each of these two types of flame can be further divided into five flame structures as shown from Figs. 2c–2g. The authors define them as ring flame, truncated open flame, dual-structure triple-layer flame, momentum-controlled yellow tip flame and momentum-controlled yellow plume flame. A clear flame neck is found in the first four types of flame. This flame neck is formed when the air/fuel jets interaction is strong. Firstly, the air velocity should be large enough to produce large enough negative pressure. Secondly, the velocity difference between the air/fuel jets should be large enough to create sufficient pressure difference between them to facilitate the deflection and impingement of the fuel jets. When these two conditions are met,

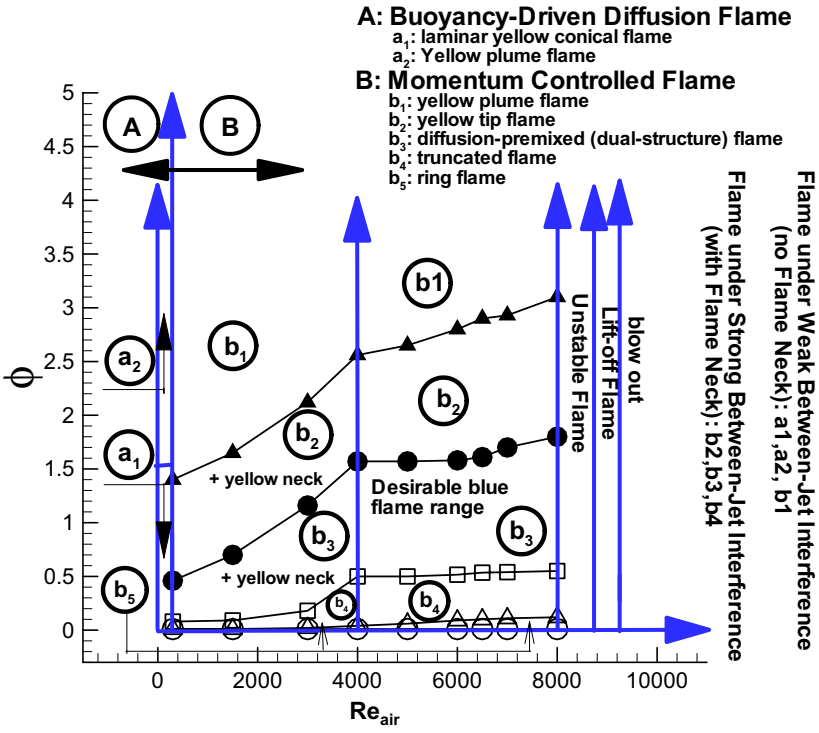

Fig. 4. Operation range of the IDF.

the fuel jets will redirect themselves towards the air jet, and eventually impinge on it causing an intense mixing. The flame neck formed due to the changed flow filed is also observed by other investigators [56]. It can be further observed that the primary difference of these momentum-controlled flames from those buoyancy-driven ones lies in that they only have one outer flame layer. No inner layer flame attached to the air jet exit is found. This is due to the increased quench effect of the cold air jet when Re_{air}, and equivalently, the air jet flow rate, is high enough. The corresponding schematic structures of these flames are shown from Figs. 3c–3g.

Actually, the impinging fuel jets acts as cross-flow for the air jet. The high pressure formed around the stagnation point creates a recirculation zone, which stabilizes the premixed flame formed at the flame neck. The stabilization effect of this impingement-induced recirculation zone is proved to be very effective, which is able to guarantee a wide stable range of flame operating conditions. The flame remains stable until Re_{air} reaches 8000. The upper premixed flame starts to lift off from the flame neck when Re_{air} is increased to 8800, and finally the whole flame blows out when Re_{air} reaches 9300.

Ring flame is named because it looks like a blue ring when viewed from the top with a hollow circular hole in the center, as shown in Figs. 2c and 3c. It is actually the base flame with no flame propagating beyond the neck. Fig. 4 shows that the ring flame is formed in the extreme fuel-lean conditions with Φ less than 0.2. The ring flame is formed because the majority of the fuel has been consumed when it reaches the flame neck. So no flame is developed further downstream. When Φ is increased, there is unburned fuel reaching the flame neck and mixes there with the air jet. The mixed fuel and air will march downstream as a partially premixed flame. The flame temperature and species emission profiles to be presented later will further confirm this partially premixed combustion.

When we further increase Φ to a value below 0.4 for the stable range of Re_{air}, an truncated premixed flame with an open flame tip is formed, as shown in Figs. 2d and 3d. This type of flame structure is classified as open flame. Fuel is mixed and burned with the air at the periphery of the air jet, resulting in the open flame.

A complete premixed flame appearance is exhibited when more fuel is provided after Φ exceeds a certain value under different Re_{air}, as shown in the b_3 region in Fig. 4 This is a dual-structure, triple-layer flame with a flame base and a premixed flame torch connected by the flame neck. Both diffusion and premixed flame structures (dual-structure) are found in this type of IDF, with the base flame being a diffusion one and the flame torch a premixed one. The upper premixed flame comprises a deep blue inner reaction cone and a pale blue outer layer of post-combustion products, together with the base flame, three layers of flame are found in this IDF. The image of the flame is shown in Figs. 2e and 3e.

When Φ is further increased, soot starts to form in the region around the flame tip, which is defined as yellow tip flame, as shown in Figs. 2f and 3f. The long diffusion outer flame length increases the residence time, thus facili-

tating the formation of soot at the end of the flame tip. The transition points from blue dual-structure triple-layer IDF to yellow tip flame is shown in the lines separating the regions b_2 and b_3 in Fig. 4.

When Φ is further increased and exceeds a certain value, the yellow flame spreads from the top downwards and eventually occupies nearly the whole flame, leaving only a short base flame. The flame neck and the inner cone of the premixed flame disappear. A typical turbulent yellow diffusion flame emerges, as shown in Figs. 2(g) and 3(g). In this flame, the velocity difference between the air and fuel jets is too small to alter the trajectory of the fuel jets. In fact, the air jet velocity has a negligible influence on the flow field and flame structure. It is the fuel jet velocity that dominates the flow and combustion characteristics, causing a typical turbulent diffusion flame appearance.

Thus far, we have seen how the fuel/air jets interference level dominates the flame structure. A desirable flame structure has to be determined. It is observed that the dual-structure triple-layer IDF is all blue when Re_{air} is larger than 4000. This IDF combines the advantages of both diffusion and premixed combustion. The base flame is a diffusion one with no danger of flashback. The upper flame torch is a turbulent premixed one with high heat release rate. The IDF remains stable until $Re_{air} = 8000$. This self-stability feature enables the IDF to possess a satisfactory stability limit without any external means. Therefore, this all blue IDF has good potential for heating purpose including the application for domestic use. The emphasis of the present study is put on this type of IDF. It is observed from Fig. 2e that the flame base is short and laminar. The inner reaction zone of the premixed flame is wrinkled, thickened, and brush-like, indicating a fully turbulent combustion. The outer layer of the premixed flame is very long due to the large global equivalence ratio ($\phi = 1.8$) with more post-combustion reaction along the way. It will be shown later in Fig. 5(c) that the total length of the flame will reduce dramatically with decreasing Φ. This facilitates an easy control of the flame length by varying Φ.

The desirable flame structure has been ascertained to be blue, dual-structured, and triple-layered, which combines the advantages of premixed and diffusion flames. It is featured with a wide stabilization range, high heat release rate, and easily controllable flame length. For this reason, the following investigation and discussion will focus on this type of IDF. The values of the relevant parameters are selected to be in the range where the blue, dual-structure, triple-layer IDF is produced according to the flame stability chart provided in Fig. 4.

4.2. Flame height

The flames discussed here are observed to be blue on the whole. It is found that considerable errors will be caused if we measure the flame length from the direct photos because of the transparency. Therefore, flame heights are ascertained by direct measurement from the flame through visual observation in the present study. Determining the blue flame height by visual observation is a widely used method [57]. The distinctly stable dual flame structure makes it easy to identify visually the deep blue or green inner reaction cone and the pale blue outer layer. A total five sets of measurement have been made, and a good duplication is found between each set with minimum and maximum error of 2.3% and 11.7%, respectively. The effects of the two key parameters, i.e., Re_{air} and Φ, on the variation of flame length, are examined and shown from Fig. 5a–c.

Fig. 5a shows the height of the flame at each layer when Re_{air} is varied from 1000 to 8000 under the same air/fuel velocity ratio at $\phi = 1$. Fig. 4 shows that the flames considered will progress from a yellow neck, yellow tip flame to a yellow neck, dual-structure triple-layer flame and finally into a dual-structure triple-layer flame without yellow neck, as Re_{air} is increased. At a fixed Φ, an increase

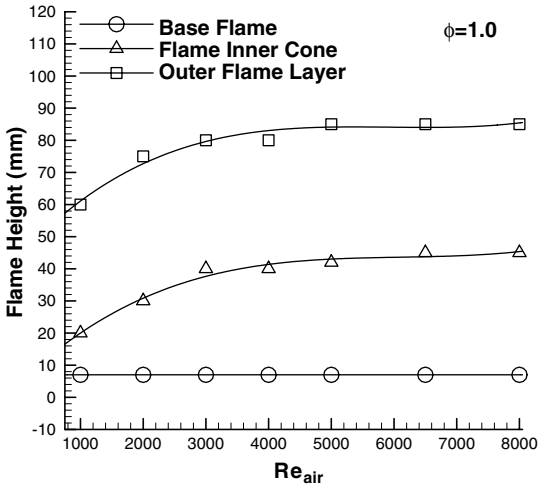

Fig. 5a. Effect of Re_{air} on flame height of the IDF at $\Phi = 1.0$.

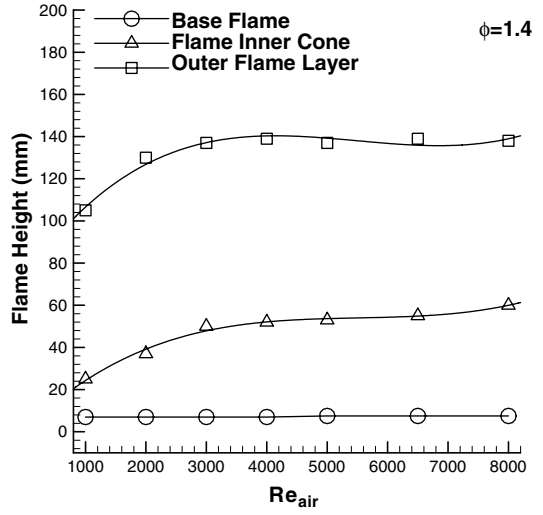

Fig. 5b. Effect of Re_{air} on flame height of the IDF at $\Phi = 1.4$.

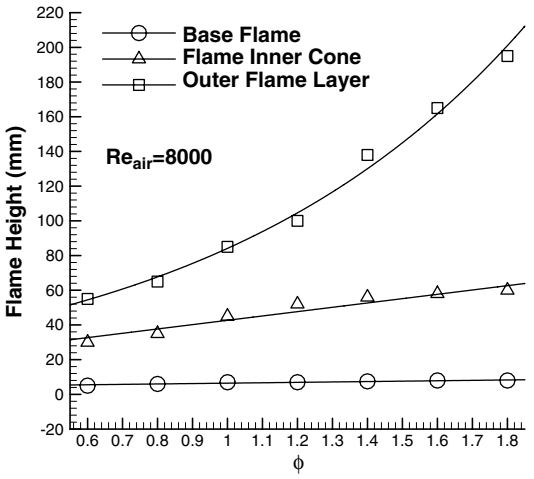

Fig. 5c. Effect of Φ on flame height of the IDF at $Re_{air} = 8000$.

in Re_{air} means a corresponding increase in the fuel supply with an increase in the air supply.

In Fig. 5a, the length of the base flame is short and its length remains constant at 7 mm. In contrast, the base flame length increases gradually and slightly from 5 mm to 8 mm when Φ is increased from 0.6 to 1.8 as shown in Fig. 5c. It is shown in Fig. 5a that the lengths of both the inner reaction zone and the outer layer of the flame increase with Re_{air}. When Re_{air} is less than 3000, the rate of increase is large, indicating strong dependence of the flame length on Re_{air}. However, when Re_{air} is above 3000, this dependency turns out to be much weaker. When a yellow-tipped b_2 flame moves towards higher Re_{air} at $\Phi = 1$, the corresponding increase in fuel will lengthen the flame while the increase in air/fuel mixing will shorten the flame. The net result is an increase in flame length at a low level of $Re_{air} < 3000$. There is a progressive shortening of the yellow tip region as Re_{air} is increased indicating stronger air/fuel mixing which tends to shorten the flame. Stronger fuel entrainment occurs at higher Re_{air} leading to the formation of dual-structure, triple-layer flames. The stronger entrainment force also sucks atmospheric air into the flame to support premixed combustion. Thus despite an increase in fuel supply, there is no obvious increase in flame length.

Similar variation of the flame length with Re_{air} is obtained at $\Phi = 1.4$, as shown in Fig. 5b. However, the height of the inner cone and the height of the outer flame layer are larger than those of the corresponding flame at $\Phi = 1.0$. Thus far, we can conclude that for a blue dual-structure triple-layer flame, Re_{air} has negligible influence on the total flame length, i.e., the height of the outer flame layer. The total flame height is almost solely dependent on Φ. This Re_{air}-independency suggests that the flame is self-similar in this region. This may due to the self-similar flow in this range of Re_{air}. Based on this finding, we select only one Re_{air} of 8000 to investigate the influence of Φ on the flame length.

The influence of Φ on the heights of the premixed flames, as shown in Fig. 5(c), is quite different from that of Re_{air}. At Re_{air} of 8000, when Φ is increased from 0.6 to 1.8, Fig. 4 shows that the flames considered will progress from a dual-structure triple-layer flame to a yellow tip flame. At a fixed Re_{air}, when Φ is increased, the air supply remains constant but the fuel supply is increased, leading to an increase in the flame length. This is especially true when the flame becomes a yellow tip flame at $\Phi > 1.5$. There is an increase in the yellow tip as Φ is increased towards 1.8, indicating an increasing amount of fuel burned in the diffusion mode.

Fig. 5c shows that the inner cone length increases gradually and almost linearly with increasing Φ, stretching from fuel-lean ($\Phi = 0.6$), to fuel-rich ($\Phi = 1.8$) conditions. This is because more fuel provided with larger Φ needs to be consumed in a longer flame, even in the premixed mode. The linear correlation is expressed as follows:

$$L_{f,inner} = 29.3\phi + 13.9 \quad (1)$$

It can be seen from Fig. 5c that the height of the outer layer of the premixed flame is very sensitive to Φ, which increases exponentially with increasing Φ. This sharp increase in the length of the flame outer layer is attributed to the diffusion combustion mechanism especially in the yellow-tipped region. Long flame length is one of the inherent characteristics of diffusion combustion. The exponential relationship between the flame length and Φ is correlated as:

$$L_{f,outer} = 27.4e^{1.1\phi} \quad (2)$$

The flame length correlates inherently to the thermal and emission characteristics of the flame. We will discuss this relevance in the following section.

4.3. Thermal characteristics

The thermal behavior of the blue dual-structure triple-layer IDF is examined by flame temperature measurement.

4.3.1. Flame temperature distribution

The temperature contour is shown in Fig. 6a. Four typical thermal zones are identified. Below the flame neck is the base flame zone, where the temperatures are relatively low. The base flame comprises a cold central core which is located in the potential core region of the air jet. Beyond the flame neck, the temperature increases gradually in the mixing zone. The cool core still exists, which is due to the existence of the excess air in the center. The mixing of fuel and air is finally completed in this region before it reaches the turbulent reaction zone which starts approximately from $y = 32$ mm. This location is in good agreement with what we have observed visually as the bottom boundary of the reaction zone. In the reaction zone, the cool central region disappears completely. The upper boundary of the reaction zone is set to be the midpoint of the maximum flame temperature (T_f), which is around $y = 58$ mm in this

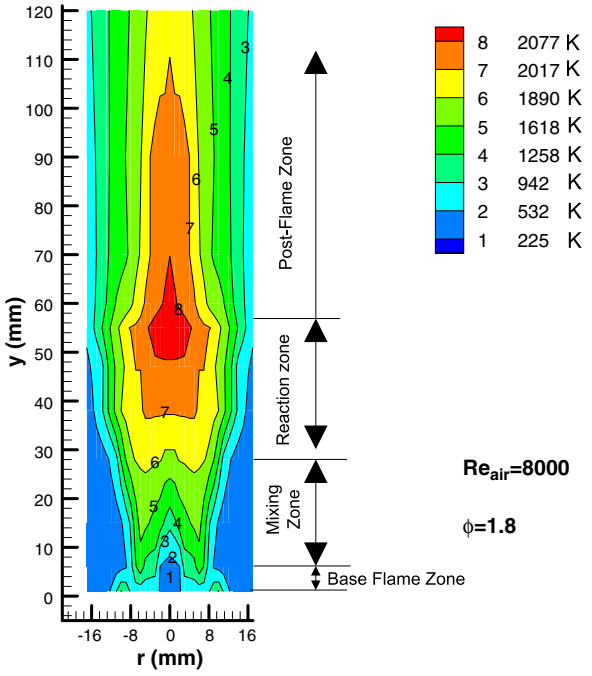

Fig. 6a. Temperature Contour of the IDF at $Re_{air} = 8000$ and $\Phi = 1.8$.

flame. This is very close to the visually observed height of the reaction zone −60 mm. The post-flame zone is characterized by a long high-temperature region, where complete combustion is achieved. This long high-temperature post-flame zone together with the high-temperature reaction zone makes the IDF highly desirable for heating application.

The variations of the centerline temperature with Re_{air} are shown in Fig. 6b where two distinct regions can be identified. When y is less than around 92 mm, the temperatures vary almost along the same trend line for Re_{air} of 4000 to 8000. T_f increases at a fast pace in the mixing zone until it reaches 2000 K at around $y = 32$ mm in the reaction zone. After that, a high-temperature plateau stretches to the post-flame zone at around 92 mm. This temperature similarity under different Re_{air} corresponds to the similarity found in the flame height, which suggests a possible self-similar flow in this region. When y is larger than 92 mm, the temperature under higher Re_{air} declines a little bit faster. This is because of the stronger entrainment of the surrounding air under higher Re_{air} due to higher turbulence level. The entrained air dilutes and cools the flue gas.

The distribution of T_f with Φ is shown in Fig. 6c where Φ is varied from fuel-lean to fuel-rich conditions. It is observed that for the fuel-lean conditions, the flame temperatures increase dramatically with increasing Φ. The maximum temperatures are 790 K, 1292 K, and 1795 K under the conditions of $\Phi = 0.6$, $\Phi = 0.8$, and $\Phi = 1.0$, respectively. Each of them is below the adiabatic flame temperature, which indicates fuel-lean combustion in the upper premixed flame. In each case, T_f increases fast first to the peak value and then decreases gradually. No high-temperature plateau is formed. This indicates that no major combustion occurs in the post-flame zone. Fuel has been consumed completely in the reaction zone, leaving the post-flame zone only characterized by entrainment and dilution, and thus the gradual reduction in flue gas temperature. For the fuel-rich conditions with $\Phi = 1.4$ and $\Phi = 1.8$, the peak flame temperatures are similar to each other, approaching around 2100 K. A high-temperature plateau follows the temperature peak. This high-temperature plateau straddles the reaction and post-flame zones. The existence of combustion in the post-flame zone suggests a fuel-rich premixed combustion as a whole. Therefore, we can conclude that high-temperature IDF is produced only in the fuel-rich conditions. Combustion of fuel and air with a stoichiometric or fuel-lean global equivalence ratio will lead to a dramatic decrease in flame temperature, which is less desirable for heating purpose.

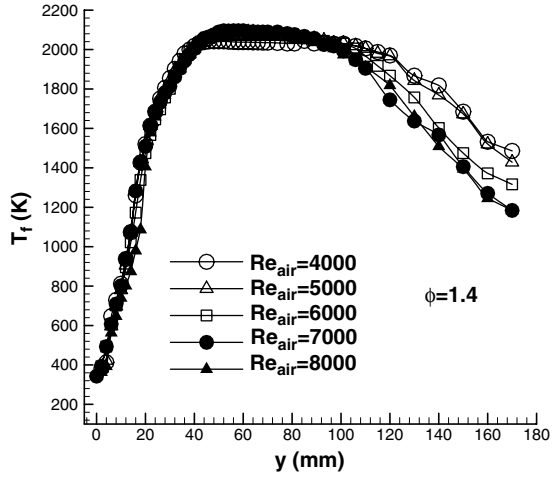

Fig. 6b. Effect of Re_{air} on the flame temperature distribution along the centerline.

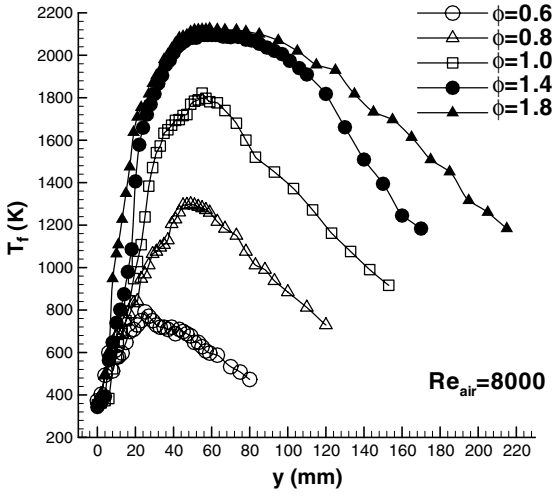

Fig. 6c. Effect of Φ on the flame temperature distribution along the centerline.

4.3.2. Species concentration distribution

To further understand the flame structure, the distributions of the combustion species concentrations within the flame were investigated and the results are shown from Fig. 7a–d, for $Re_{air} = 8000$ and $\Phi = 1.8$. The distributions of the species concentrations along the flame centerline can be divided into five characteristic regions: base flame region, pre-combustion region, combustion region, post-flame species conversion region (where the majority of the incomplete combustion-produced species such as CO and HC are consumed and converted to complete combustion products), and post-flame entrainment region (which is mainly featured with pure entrainment). It is observed from Fig. 7a that in the base flame region where $y \leqslant 8$ mm, the concentrations of O_2 is 20.9% and no CO_2 is found. This indicates that the air in the center does not yet meet the surrounding fuel jets, and thus no combustion occurs. In the pre-combustion zone, the concentration of CO_2 increases sharply, while the concentration of O_2 decreases sharply at the same time. Both of these sharp variations stop at around $y = 32$ mm, which is the bottom point of the turbulent reaction zone. After that, the concentration of O_2 decreases slightly and gradually until $y = 80$ mm. Meanwhile, the concentration of CO_2 maintains at a stable level in this region. This region stretches from the reaction zone to the early post-flame zone as defined by the flame temperature shown in Fig. 6a. The stable levels of concentrations indicate very little entrainment of the surrounding air in this region. This further confirms indirectly that this is a heat release-dominant region. On one hand, heat release suppresses entrainment according to Han and Mungal [47]. On the other hand, the boundary layer of the reaction zone acts as a barrier hindering the encroachment of the surrounding air. As a result, the flame center is undisturbed. The fourth region extends from $y = 80$ mm to $y = 125$ mm, where the CO_2 concentration increases again axially and the O_2 concentration also

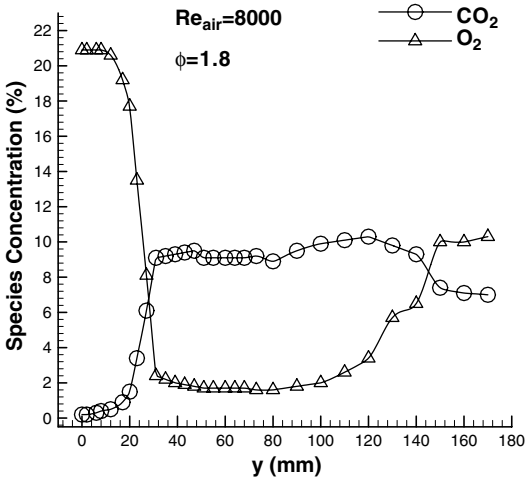

Fig. 7a. Distribution of CO_2 and O_2 concentrations along the centerline at $Re_{air} = 8000$ and $\Phi = 1.8$.

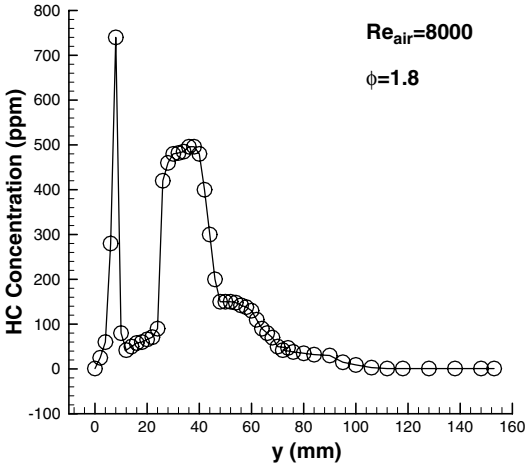

Fig. 7b. Distribution of HC concentrations along the centerline at $Re_{air} = 8000$ and $\Phi = 1.8$.

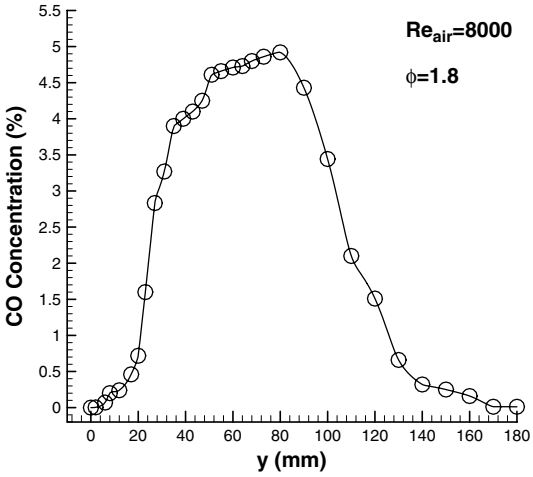

Fig. 7c. Distribution of CO concentrations along the centerline at $Re_{air} = 8000$ and $\Phi = 1.8$.

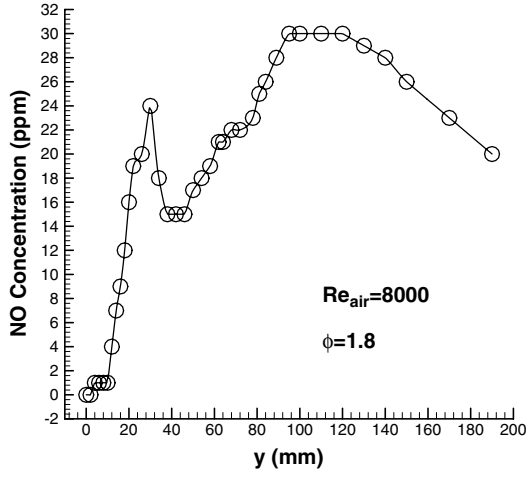

Fig. 7d. Distribution of NO concentrations along the centerline at $Re_{air} = 8000$ and $\Phi = 1.8$.

increases at the same time. This part of post-flame region is featured with buoyancy-driven flame flickering. According to Han and Mungal [47], buoyancy could accelerate the entrainment, resulting in the increase in O_2 concentration. It is predicted at this moment that the increase in CO_2 is attributed to the conversion of CO with the entrained inflowing air. Thus, we can conclude that the combustion process is finally completed in this region. The fifth and last region follows afterwards with $y > 125$ mm. This region is characterized by pure entrainment without reaction activity. Due to entrainment, the concentration of CO_2 starts to decline and the O_2 concentration starts to increase.

The distribution of HC concentration is shown in Fig. 7b. In the base flame region, the HC concentration increases from zero to a peak in the flame neck. When the fuel jets impinge on the cold air jet, partial quenching will occur, giving rise to this peak emission of HC. Beyond the flame neck, the HC concentration decreases sharply first and then increases gradually in the pre-combustion zone until $y = 32$ mm. The re-increase in HC concentration indicates the incomplete combustion. In the following reaction zone, the HC concentration declines gradually to 35 ppm until $y = 80$ mm. This HC concentration continues to decline in the post-flame species conversion region and is finally completely consumed there.

The CO concentration distribution is shown in Fig. 7c. It is observed that in the base flame zone, the CO concentration is very low. The CO concentration increases quickly in the pre-combustion zone due to the increased flame temperature. In the reaction zone, the CO concentration increases slowly and on the whole remains at a high level of 3.6–4.92%. This high level of CO in the reaction zone indicates a fuel-rich combustion. Wu and Essenhigh [58] also reported a large amount of CO of over 6% near the flame tip in a concentric IDF. We can further observe from Fig. 7c that the high level CO concentration decreases sharply in the post-flame region. This is because CO is consumed with the entrained air and converted to CO_2 in this region, leaving only a small amount of CO as a net emission. This claim can be validated by the increased CO_2 concentration shown in Fig. 7a. In contrast, Sidebotham and Glassman [57] found that the CO was formed on the fuel side and did not penetrate across the reaction zone for further oxidation, but convected radially outwards as net emission. Leonard et al. [59] also presented a hypothesis that IDFs emit large amount of CO in a manner similar to under-ventilated NDFs. This divide in the CO emission is very likely due to different flame structure and combustion pattern, with the flame in the present study being actually acting as premixed flame. In the post-flame entrainment region, the CO concentration declines further due to entrainment and reaches 115 ppm at $y > 170$ mm as an emission.

The NO concentration distribution is shown in Fig. 7d. The NO level in the base flame region is very low. Then it increases dramatically in the pre-combustion region to a peak value of 24 ppm. In the reaction zone, the NO concentration decreases first until $y = 40$ mm, and then increases steadily. The NO concentration continues to increase in the post-flame zone till $y = 125$ mm, where complete combustion is achieved. Referring back to the temperature distribution in Fig. 6c, we can find that this region is featured with flame temperature higher than 1900 K. Thus the thermal NO could be the dominant NO formation mechanism in this region. This thermal NO-dominant mechanism is also reported by other investigators. Correa [60] found that NO formation occurred primarily in the region of the IDF tip where it is conducive to NO formation via temperature sensitive mechanism due to a combination of high temperatures and large residence times, which suggests dominance by the thermal-NO mechanism. Partridge et al. [41] presented spatially resolved, LSF measurement of NO in IDF and found that the majority of the IDF-attributable NO is generated at the IDF tip. In the post-flame entrainment zone, the NO concentration decreases monotonically due to air dilution.

4.4. Pollutants emission

The net emissions of CO, NO and NO_x on dilution air-free basis are presented in Fig. 8a. It is found that the [CO] decreases with the increase in Φ, while the variations of [NO] and [NO_x] follow the inverse trend. When Φ is lower, the quenching effect of the excess central cold air on the flame lowers the flame temperature, as shown in Fig. 6c, and thus increasing the CO emission. On the other hand, the steadily increasing flame temperature with the increase in Φ prompted the emission of NO and NO_x. To facilitate the comparison of the present study with the previous studies, emission index (EI) is used. The EI emissions of CO, NO and NO_x are shown in Fig. 8b. It can be seen that the variations of EICO, EINO and $EINO_x$ follow the same trend line as those of [CO], [NO] and [NO_x]. It is found from Fig. 8b that the maximum EINO and $EINO_x$ are 1.2 and 2.8, respectively. This emission level is similar to

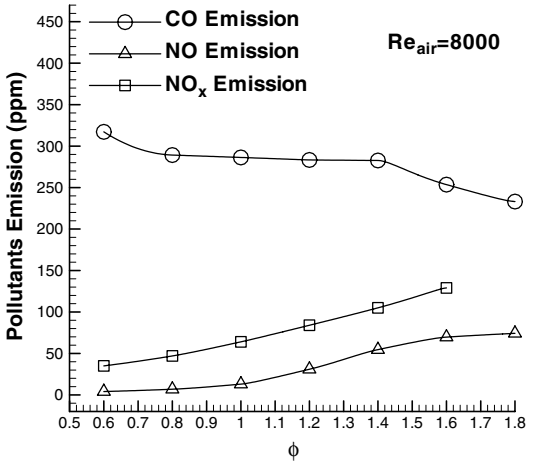

Fig. 8a. Pollutants emissions on air-free basis.

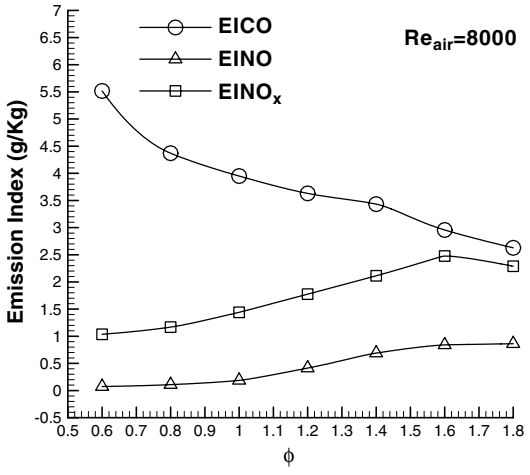

Fig. 8b. Emission index of the CO, NO and NO_x.

that in the partially premixed flame reported by Lyle et al. [61], where the maximum EINO and $EINO_x$ from the partially premixed flame are around 1.5 and 2.5, respectively when $\phi = 1.0$. The maximum EINO and $EINO_x$ are 2.4 and 2.5 from the inverse diffusion flame in air-staged burner studied by Partridge and Laurendeau [41]. For air-staged diffusion flame, Stansel et al. [62] reported that the maximum $EINO_x$ reaches 2.8. Therefore, we can conclude that low NO_x emission is another favorable characteristics of the IDF we are studying.

5. Conclusions

The flow pattern, flame structure and pollutants emission characteristics of an inverse diffusion flame jet have been investigated experimentally to explore the feasibility for impingement heating. The following conclusions can be drawn from this investigation:

1. The interference between air and fuel jets complicates the flow pattern and determines the flame structure. It is found that the flame shape and structure are mainly dependent on the air jet velocity and the ratio of the air and fuel velocities. In the present study, these two factors are equivalent to Re_{air} and Φ. With varying Re_{air} and Φ, seven flame structures are identified. Among them, the blue dual-structure triple-layer flame contains a base diffusion flame and a flame torch connected by the flame neck. The flame torch is like a premixed flame with an inner reaction zone and an outer flame layer. It is found that it is this type of IDF that combines the advantage of both diffusion flame and premixed flame, with no possibility of flashback, high flame temperature and acceptable pollutants emission level.
2. The thermal structure of the IDF can be divided into four characteristic zones, i.e., the base flame zone, which is cool and lack in chemical reaction, the mixing zone, which includes the flame neck where the fuel/air mixing is completed, the combustion zone, which refers to the inner cone, and the post-flame zone. The post-flame zone is characterized by chemical reaction in the early stage and air dilution in the latter. The peak T_f increases with O until $\phi = 1.4$. After that, the peak T_f remains stable. The peak T_f is found to change little with Re_{aur}, manifesting a self-similarity. Thus high flame temperature can only be obtained with $\phi > 1.4$.
3. The IDF can be self-stabilized in a wide range of Re_{air} and Φ. It remains stable without external facility up to $Re_{air} = 8000$. It blows out when $Re_{air} = 8800$. This good flame stability is attributed to its special flame structure. The surrounding fuel jets impinge on the central air jet when the velocity difference is large enough. The high pressure around the stagnation point results in the formation of a recirculation zone near the flame neck, which stabilizes the premixed flame torch.
4. Among the seven structures of the IDF, the blue dual-structure triple-layer IDF is singled out as a desirable option for impingement heating because of the combination of both premixed and diffusion flame jets, i.e., high flame temperature, less or no soot emission, and acceptable pollutants emission level. Furthermore, the excellent self-stabilization capability in large Re_{air} of the IDF makes it more advantageous than premixed or partially premixed flame jets in terms of flame stabilization. Therefore, this IDF has the great potential in impingement heating. The further investigation on the characteristics of impingement heat transfer is presented in the second part of this paper.
5. The [CO] and EICO decrease with the increase in Φ, while [NO], [NO_x], EINO, $EINO_x$ increase accordingly. This is mainly due to the monotonic increase in T_f with Φ. The IDF in the present study emits a comparable level of NO and NO_x with those from partially premixed flame and air-staged burner. Therefore, the IDF burner we are using could be attributed to low-NO_x burner.

Acknowledgements

The authors wish to thank The Hong Kong Polytechnic University and the Research Grants Council of the Hong Kong SAR (Project No. PolyU 5142/05E) for financial support of the present study.

References

[1] C.J. Hoogendoorn, Cz.O. Popiel, Th.H. van der Meer, Turbulent heat transfer on a plane surface in impingement round premixed plate jets, Int. Heat Transfer Conf. (1978) 107–112.
[2] E. Buhr, G. Haupt, H. Kremer, Heat transfer from impinging turbulent jet flames to plane surfaces, Combust. Inst. Eur. Symp. (1973) 607–612.
[3] J.E. Anderson, E.F. Stresino, Heat transfer from flames impinging on flat and cylindrical surfaces, J. Heat Transfer 85 (1963) 49–54.
[4] R. Viskanta, Heat transfer to impinging isothermal gas and flame jets, Exp. Thermal Fluid Sci. 6 (1993) 111–134.

[5] R. Viskanta, Convective and radiative flame jet impingement heat transfer, The Ninth International Symposium on Transport Phenomena in Thermal-Fluids Engineering (1996) 46–60.
[6] C.E. Baukal, B. Gebhart, A review of flame impingement heat transfer studies – Part 1: Experimental conditions, Combust. Sci. Technol. 104 (1995) 339–357.
[7] C.E. Baukal, B. Gebhart, A review of flame impingement heat transfer studies – Part 2: Measurements, Combust. Sci. Technol. 104 (1995) 359–385.
[8] C.E. Baukal, B. Gebhart, A review of semi-analytical solutions for flame impingement heat transfer, Int. J. Heat Mass Transfer 39 (14) (1995) 2989–3002.
[9] C.E. Baukal Jr., B. Gebhart, A review of empirical flame impingement heat transfer correlations, Int. J. Heat Fluid Flow 17 (1996) 386–396.
[10] S. Chander, A. Ray, Flame impingement heat transfer: a review, Energy Convers. Manage. 46 (18–19) (2005) 2803–2837.
[11] J.K. Kilham, M.R.I. Purvis, Heat transfer from hydrocarbon–oxygen flames, Combust. Flame 16 (1971) 47–54.
[12] J.K. Kilham, M.R.I. Purvis, Heat transfer from normally impinging flames, Combust. Sci. Technol. 18 (1978) 81–90.
[13] J.S. Becker, L.K. Farmer, Rapid fire heating system used oxy-gas burners for efficient metal heating, Indust. Heating (1995) 74–78.
[14] R. Conolly, R.M. Davies, A study of convective heat transfer from flames, Int. J. Heat Mass Transfer 15 (1973) 2155–2172.
[15] T.H. van der Meer, Stagnation point heat transfer from turbulent low Reynolds number jets and flame jets, Exp. Thermal Fluid Sci. 4 (1991) 115–126.
[16] A. Milson, N.A. Chigier, Studies of methane and methane–air flames impinging on a cold plate, Combust. Flame 21 (1973) 295–305.
[17] J.E. Hustad, O.K. Sonju, Radiation and size scaling of large gas and gas/oil diffusion flames, AIAA Progress Astronaut. Aeronaut. 105 (1986) 365–387.
[18] L.L. Dong, C.S. Cheung, C.W. Leung, Heat transfer from an impinging premixed butane/air slot flame jet, Int. J. Heat Mass Transfer 45 (5) (2002) 979–992.
[19] K. Kataoka, H. Shundoh, H. Matsuo, Convective heat transfer between a flat plate and a jet of hot gas impinging on it, Drying 84 (1984) 218–227.
[20] K. Kataoka, Optimal nozzle-to-plate spacing for convective heat transfer in nonisothermal, variable-density impinging jets, Drying Technol. 3 (2) (1985) 235–254.
[21] G.K. Hargrave, M. Fairweather, J.K. Kilham, Forced convective heat transfer from premixed flames – Part 1: Flame structure, Int. J. Heat Fluid Flow 8 (1) (1987) 55–63.
[22] G.K. Hargrave, M. Fairweather, J.K. Kilham, Forced convective heat transfer from premixed flames – Part 1: Impingement heat transfer, Int. J. Heat Fluid Flow 8 (2) (1987) 132–138.
[23] Theo van der Meer, Heat transfer from impinging flame jets, Ph.D. Thesis, 1987, the Delft University, Netherland.
[24] H. Kremer, E. Buhr, R. Haupt, Heat Transfer from Turbulent Free-Jet Flames to Plate surfaces (1973) 463–472.
[25] L.L. Dong, C.W. Leung, C.S. Cheung, Heat transfer characteristics of premixed butane/air flame jet impinging on an inclined flat surface, Heat Mass Transfer 39 (2002) 19–26.
[26] S.G. Tuttle, B.W. Webb, M.Q. Mcquay, Convective heat transfer from a partially premixed impinging flame jet. Part 1: Time-averaged results, Int. J. Heat Mass Transfer 48 (7) (2005) 236–1251.
[27] S.G. Tuttle, B.W. Webb, M.Q. Mcquay, Convective heat transfer from a partially premixed impinging flame jet. Part 2: Time-resolved results, Int. J. Heat Mass Transfer 48 (7) (2005) 1252–1266.
[28] L.L. Dong, C.W. Leung, C.S. Cheung, Heat transfer and wall pressure characteristics of a twin premixed butane/air flame jets, Int. J. Heat Mass Transfer 47 (3) (2004) 489–500.
[29] L.L. Dong, C.W. Leung, C.S. Cheung, Heat transfer of a row of butane/air flame jets impinging on a flat plate, Int. J. Heat Mass Transfer 46 (2003) 113–125.
[30] S. Chander, A. Ray, Heat transfer characteristics of three interacting methane/air flame jets impinging on a flat surface, Int. J. Heat Mass Transfer 50 (3–4) (2007) 640–653.
[31] G.K. Malikov, D.L. Lobanov, Y.K. Malikov, V.G. Lisienko, R. Viskanta, A.G. Fedorov, Experimental and numerical study of heat transfer in a flame jet impingement system, J. Inst. Energy 72 (1999) 2–9.
[32] J.W. Mohr, J. Seyed-Yagoobi, R.H. Page, Heat transfer characteristics of a radial jet reattachment flame, J. Heat Transfer 119 (1997) 258–264.
[33] J. Seyed-Yagoobi, V. Narayanan, R.H. Page, Comparison of heat transfer characteristics of radial jet reattachment nozzle to in-line impinging jet nozzle, J. Heat Transfer 120 (1998) 335–341.
[34] J. Wu, J. Seyed-Yagoobi, R.H. Page, Heat transfer and combustion characteristics of an array of radial jet reattachment flames, Combust. Flame 125 (2001) 955–964.
[35] J.R. Rigey, B.W. Webb, An experimental investigation of diffusion flame jet impingement heat transfer, Proc. ASME/JSME Thermal Eng. Joint Conf. 3 (1995) 117–126.
[36] M. Fairweather, J.K. Kilham, A. Mohebi-Ashtiani, Stagnation point heat transfer from turbulent methane–air flames, Combust. Sci. Technol. 35 (1984) 225–238.
[37] M.R.I. Purvis, Heat transfer from normally impinging hydrocarbon oxygen flames, Ph.D. Thesis, 1974, University of Leeds.
[38] L.G. Blevins, G.W. Mulholland, R.W. Davis, Carbon monoxide and soot formation in inverse diffusion flames, Fifth International Microgravity Combustion Workshop (1999).
[39] K.C. Oh, U.D. Lee, H.D. Shin, E.J. Lee, The evolution of incipient soot particles in an inverse diffusion flame of ethene, Combust. Flame 140 (2005) 249–254.
[40] C.R. Shaddix, T.C. Williams, L.G. Blevins, R.W. Schefer, Flame structure of steady and pulsed sooting inverse jet diffusion flames, Proc. Combust. Inst. 30 (2005) 1501–1508.
[41] W.P. Partridge, N.M. Laurendeau, Nitric oxide formation by inverse diffusion flames in staged-air burners, Fuel 74 (10) (1995) 1424–1430.
[42] B. Fleck, Experimental and Numerical Investigation of the Novel Low-NO_x Industrial Burner, Ph.D. Thesis, Queen's University, 1998.
[43] D. Bradley, K.J. Matthews, Measurement of high gas temperatures with fine wire thermocouple, J. Mech. Eng. Sci. 10 (1968) 299–305.
[44] E.M. Sparrow, R.D. Cess, Radiation heat transfer, augmented edition., McGraw-Hill, New York, 1978.
[45] S.J. Kline, F.A. McClintock, Describing uncertainties in single sample experiments, Mech. Eng. 75 (3–8) (1953).
[46] A. Sinha, R. Ganguly, I.K. Puri, Control of confined nonpremixed flames using a microjet, Int. J. Heat Fluid Flow 26 (2005) 431–439.
[47] D. Han, M.G. Mungal, Direct measurement of entrainment in reacting/nonreacting turbulent jets, Combust. Flame 124 (2001) 370–386.
[48] D.B. Bain, C.E. Smith, Mixing analysis of axially opposed rows of jets injected into confined crossflow, J. Propulsion Power 11 (5) (1995) 885–893.
[49] D.J. Holve, R.F. Sawyer, Diffusion controlled combustion of polymers, Presented at the 15th International Symposium on Combustion (1974).
[50] P.O. Witze, A study of impinging axisymmetric turbulent flows: the wall jet, the radial jet, and opposing free jets, SAND 74-8257 (1975).
[51] S.R. Turns, An introduction to combustion: concepts and applications, McGraw-Hill, Inc.,, 2000.
[52] A. Hamins, J.C. Yang, T. Kashiwagi, An experimental investigation of the pulsation frequency of flames, Proc. Combust. Inst. 24 (1992) 1695–1702.
[53] R.F. Huang, J.T. Yang, P.C. Lee, Flame and flow characteristics of double concentric jets, Combust. Flame 108 (1997) 9–23.
[54] I. Kimura, Stability of laminar jet flames, Proc. Combust. Inst. 10 (1965) 1295–1300.
[55] Z. Shu, S.K. Aggarwal, V.R. Katta, I.K. Puri, Combust. Flame 111 (1997) 276–286.

[56] A. Sobiesiak, J.C. Wenzell, Characteristics and structure of inverse flames of natural gas, Proc. Combust. Inst. 30 (2005) 743–749.
[57] G.W. Sidebotham, I. Glassman, Flame temperature, fuel structure and fuel concentration effects on soot formation in inverse diffusion flames, Combust. Flame 90 (1992) 269–283.
[58] K.T. Wu, R.H. Essenhigh, in: Proceedings of the Combustion Institute, vol. 20, the Combustion Institute, 1984, pp. 1922–1932.
[59] S. Leonard, G.W. Mulholland, R. Puri, R.J. Santoro, Generation of CO and smoke during underventilated combustion, Combust. Flame 98 (1994) 20–34.
[60] S.M. Correa, NO emission and major species concentrations in a co-flowing inverse diffusion flame, Combust. Sci. Technol. 87 (1992) 329–362.
[61] K.H. Lyle, L.K. Tseng, J.P. Gore, N.M. Laurendeau, A study of pollutant emission characteristics of partially premixed turbulent jet flames, Combust. Flame 116 (1999) 627–639.
[62] D.M. Stansel, N.M. Laurendeau, D.W. Senser, CO and NO_x emissions from a controlled-air burner: experimental measurements and exhaust correlations, Combust. Sci. Technol. 104 (4–6) (1995) 207–234.